Experiments on the Motion of Drops on a Horizontal Solid Surface Due to a Wettability Gradient

Nadjoua Moumen, R. Shankar Subramanian,* and John B. McLaughlin

Department of Chemical and Biomolecular Engineering, Clarkson University, Potsdam, New York 13699

Received November 13, 2005. In Final Form: January 5, 2006

Results from experiments performed on the motion of drops of tetraethylene glycol in a wettability gradient present on a silicon surface are reported and compared with predictions from a recently developed theoretical model. The gradient in wettability was formed by exposing strips cut from a silicon wafer to dodecyltrichlorosilane vapors. Video images of the drops captured during the experiments were subsequently analyzed for drop size and velocity as functions of position along the gradient. In separate experiments on the same strips, the static contact angle formed by small drops was measured and used to obtain the local wettability gradient to which a drop is subjected. The velocity of the drops was found to be a strong function of position along the gradient. A quasi-steady theoretical model that balances the local hydrodynamic resistance with the local driving force generally describes the observations; possible reasons for the remaining discrepancies are discussed. It is shown that a model in which the driving force is reduced to accommodate the hysteresis effect inferred from the data is able to remove most of the discrepancy between the observed and predicted velocities.

Introduction

In this study, a method for inducing the motion of a liquid drop placed on a solid surface, identified first by Greenspan[1] and demonstrated experimentally by Chaudhury and Whitesides,[2] is investigated. The mechanism that causes motion is a gradient in wettability on the solid surface. The resulting imbalance of forces acting at the contact line around the drop periphery leads to a driving force in the direction of increasing wettability, or decreasing contact angle.

Relevant theoretical work on this problem is reviewed in detail in Subramanian et al.,[3] and only a brief discussion of that work is given here. Theoretical descriptions of drop motion along a solid surface caused by a wettability gradient are given in Greenspan[1] and Brochard,[4] and a related problem of the thermocapillary motion of a 2D ridge is analyzed by Ford and Nadim.[5] All of the models employ the lubrication approximation, which requires that the thickness of the drop, also called the height of the drop, be small compared with the characteristic length scale of the drop's footprint. Greenspan[1] related the velocity of the contact line to the difference between the dynamic and equilibrium contact angles using a proportionality constant that is assumed to be given. Brochard considered 2D ridges as well as 3D drops and analyzed isothermal situations and those in which a temperature gradient was applied. In the isothermal case involving 3D drops, the analysis involved a local force balance normal to an element of the contact line and required that trigonometric functions of the contact angle be approximated by the leading terms in their Taylor series in order to produce a consistent framework.

In the present experiments, the contact angle can be as large as 80° at the beginning of the motion and decrease to 30° at the end. To assist in the interpretation of these experiments, Subramanian et al.[3] developed an approximate quasi-steady theoretical description of the motion of a spherical-cap drop on a solid surface with a wettability gradient that does not make the lubrication approximation. The hydrodynamic resistance was calculated for Stokes flow in the drop, modeling it as a set of differential wedges. The authors also provided an exact solution of the lubrication equations for the same problem and found that the lubrication solution was good for contact angles up to about 40°. In ref 3, the stress singularity that appears at the contact line is relieved by permitting slip to occur in a region close to the contact line, assumed to be on the order of molecular dimensions. The ratio of the length of this region to the characteristic length scale of the drop's footprint is typically a small parameter, and the authors provided an asymptotic result based on an expansion in this small parameter as well.

Now, we briefly review prior experimental studies. The motion of a drop possibly arising from a wettability gradient on a surface appears to have been qualitatively observed by Bouasse,[6] who used a temperature gradient. Temperature variations along a fluid−fluid interface also cause variations in the interfacial tension along that interface, making a thermocapillary contribution to the motion, in addition to that arising from a variation in wettability. After the appearance of Bouasse's work, no experimental observations appear to have been reported on motion caused by a wettability gradient until Chaudhury and Whitesides[2] induced the upward motion of water drops on tilted surfaces along which they had created a wettability gradient. This gradient was formed by allowing decyltrichlorosilane vapor to react with a silicon strip using a diffusion-controlled process, which was adapted from a technique developed by Elwing et al.[7] Chaudhury and Whitesides[2] stated that, for drop motion to occur, contact angle hysteresis must be less than approximately 10°. The term "contact angle hysteresis" has a long history, and the phenomenon is discussed at length in a review by Dussan.[8] In the experiments of Chaudhury and Whitesides,[2] drops of water, 1 to 2 μL in volume, were observed to move at a velocity of 1 to 2 mm/s

* To whom correspondence may be addressed: subramanian@clarkson.edu.

(1) Greenspan, H. P. *J. Fluid Mech.* **1978**, *84*, 125.
(2) Chaudhury, M. K.; Whitesides, G. M. *Science* **1992**, *256*, 1539.
(3) Subramanian, R. S.; Moumen, N.; McLaughlin, J. B. *Langmuir* **2005**, *21*, 11844.
(4) Brochard, F. *Langmuir* **1989**, *5*, 432.
(5) Ford, M. L.; Nadim, A. *Phys. Fluids* **1994**, *6*, 3183.
(6) Bouasse, H. *Capillarité et Phénomènes Superficiels*; Delagrave: Paris, 1924.
(7) Elwing, H.; Welin, S.; Askendal, A.; Nilsson, U.; Lundstrom, I. *J. Colloid Interface Sci.* **1987**, *119*, 203.
(8) Dussan V, E. B. *Annu. Rev. Fluid Mech.* **1979**, *11*, 371.

10.1021/la053060x CCC: $33.50
Published on Web 02/09/2006

uphill on a surface that was inclined at an angle of 15° with respect to the horizontal. Subsequently, Daniel et al.[9] observed a more rapid motion of water drops of comparable size (at velocities of 0.15 to 1.5 m/s) when condensation occurred on surfaces on which a wettability gradient was present. The authors suggested that the increase in velocity was likely caused by the coalescence of the drops and that the phenomenon could be used to enhance heat transfer. Daniel and Chaudhury[10] investigated the motion of small drops of ethylene glycol on surfaces with a wettability gradient. These surfaces were prepared using decyltrichlorosilane following the procedure described earlier by Daniel et al.[9] They reported drop velocities in the range of 1 to 2 mm/s for drops 1 to 2 μL in volume. Daniel and Chaudhury[10] attempted to quantify the extent of contact angle hysteresis using the size of the largest drop that does not move in the gradient. They also found that the measured velocities scaled approximately linearly with the drop radius, defined as that of the drop's circular footprint. Daniel and Chaudhury[10] proposed using a periodic force (generated using a speaker to move the surface back and forth in a periodic manner) to overcome contact angle hysteresis and reported success with this approach in significantly increasing the velocities of the drops. Subsequently, Daniel et al.[11] performed experiments using a variety of liquids, reporting results for velocities that scaled approximately linearly with the drop radius and that were enhanced considerably when the substrate was vibrated. The authors[11] provided a theoretical scaling result attributed to Brochard[4] and Daniel and Chaudhury[10] in which the velocity of the drop is multiplied by the viscosity of the fluid and divided by its surface tension (against air) to define a capillary number, which then is proportional to the product of the drop radius and the spatial gradient of the cosine of the contact angle, with a constant of proportionality α. The authors suggest that α is a constant whose value depends on the mechanism of the relaxation of the stress singularity at the three-phase contact line. From the results presented by Daniel et al.[11] for a variety of liquids, it is noted that the inferred contribution from hysteresis varies from one fluid to the next.

Suda and Yamada[12] directly measured the driving force experienced by a drop on a wettability gradient surface using a flexible glass microneedle. They determined that the driving force was consistent with their expectation based on Young's equation, which represents a tangential balance of forces at the contact line.[13] Suda and Yamada[12] suggested that the principal resistance to the motion of the drop arises from the contact line region and not from the hydrodynamic drag. To estimate the contact line resistance, they used a model similar to that proposed by Cherry and Holmes[14] and Blake and Haynes[15] even though they do not explicitly mention either of these references. Ichimura et al.[16] caused drops to move on a solid surface using photoirradiation of a monolayer covering the surface to induce wettability gradients, and Sato et al.[17] report that drops were made to move on solid surfaces in a low-gravity environment by the simultaneous use of a chemically generated wettability gradient and a temperature gradient. Bain et al.[18] have demonstrated that drops containing a chemical that can modify the wettability of the surface can propel themselves on the surface by creating a local wettability gradient on the surface, a phenomenon they label "reactive flow." A variety of follow-up studies have appeared in the literature, and an example can be found in Lee and Laibinis,[19] who used noncovalent molecular adsorption to achieve the movement of drops on patterned surfaces. Recently, Mo et al.[20] have demonstrated that drops climbing a tilted surface because of reactive wetting can move at a nearly constant velocity; these authors also included a lattice Boltzmann simulation of the experiments in their work. Finally, we mention a related situation in which a drop is placed on a surface that consists of two individually homogeneous solid surfaces. On one side of the line dividing these two surfaces, the contact angle is larger than that on the other side. Raphaël[21] provided a theoretical analysis of this problem; subsequently, Ondarçuhu and Veyssié[22] performed careful experiments on 2D drops, finding confirmation of the essential aspects of the predictions of Raphaël.[21]

Even though the scaling of the drop velocity with radius is examined in refs 10 and 11, a direct comparison of theoretically predicted velocities with experimentally measured values has not been made to date. Also, all previous authors report a single velocity for a given experiment, whereas the drop velocity should, in general, exhibit a dependence on position along the gradient because both the driving force for drop motion and the hydrodynamic resistance can vary with position. For these reasons, we performed experiments on the motion of drops of tetraethylene glycol in a wettability gradient on surfaces prepared using a technique similar to that of Daniel and Chaudhury.[10] We found that the motion of the drops in any individual experiment was complex, with a velocity that varied by an order of magnitude depending on the position of the drop along the wettability gradient, a fact that has not been reported by earlier investigators. We captured digitized video frames at a rate of up to 50 per second, which permitted us to obtain a reasonably accurate picture of the instantaneous velocity as a function of position and establish that the velocity indeed varies strongly with position. Independent measurements of the static contact angle along the wettability gradient surface were made so that the driving force experienced by a moving drop could be estimated at any given position of that drop. The hydrodynamic resistance was calculated from the model presented in ref 3. It is demonstrated here that the variation in drop velocity is a consequence of the change in driving force as well as the change in hydrodynamic resistance that occurs along a typical gradient surface. We also show that a quasi-steady description appears to be sufficient to explain the observed qualitative behavior of the drop velocities along the gradient surface and discuss possible reasons for the remaining discrepancies between the predicted and measured velocities. We demonstrate that a procedure that accounts for hysteresis effects by using the inferred threshold size of a drop that would fail to move at a given location on the gradient surface is sufficient to bring the experimental results into reasonable agreement with the predictions from the wedge model presented in ref 3.

In the following sections, we present details of the experiments and compare the experimental observations with predictions from theory, concluding with a few remarks.

(9) Daniel, S.; Chaudhury, M. K.; Chen, J. C. *Science* **2001**, *291*, 633.
(10) Daniel, S.; Chaudhury, M. K. *Langmuir* **2002**, *18*, 3404.
(11) Daniel, S.; Sircar, S.; Gliem, J.; Chaudhury, M. K. *Langmuir* **2004**, *20*, 4085.
(12) Suda, H.; Yamada, S. *Langmuir* **2003**, *19*, 529.
(13) Adamson, A. W.; Gast, A. P. *Physical Chemistry of Surfaces*, 6th ed.; Wiley: New York, 1997.
(14) Cherry, B. W.; Holmes, C. M. *J. Colloid Interface Sci.* **1969**, *29*, 174.
(15) Blake, T. D.; Haynes, J. M. *J. Colloid Interface Sci.* **1969**, *30*, 421.
(16) Ichimura, K.; Oh, S.-K.; Nakagawa, M. *Science* **2000**, *288*, 1624.
(17) Sato, M.; Araki, K.; Matsuura, M.; Hasegawa, K.; Endo, A. Proceedings of the 2nd Pan Pacific Basin Workshop on Microgravity Sciences, Pasadena, CA, 2001; Paper IF-1123.
(18) Bain, C. D.; Burnett-Hall, G. D.; Montgomerie, R. R. *Nature* **1994**, *372*, 414.
(19) Lee, S.-W.; Laibinis, P. E. *J. Am. Chem. Soc.* **2000**, *122*, 5395.
(20) Mo, G. C. H.; Liu, W.-Y.; Kwok, D. Y. *Langmuir* **2005**, *21*, 5777.
(21) Raphaël, E. *C. R. Acad. Sci. Paris, Ser. II* **1988**, *306*, 751.
(22) Ondarçuhu, T.; Veyssié, M. *J. Phys. II* **1991**, *1*, 75.

Experimental Apparatus and Procedure

Equipment. The experimental apparatus designed for this study consists of three main sections—a sample holder, an injection system, and a data acquisition system. This apparatus is assembled on a vibration-isolated optical table (Melles Griot model OBH-018/07-OTL-004). The sample holder consists of a smooth horizontal surface (45 mm × 45 mm) that is mounted on a three-axis translation stage. The assembled stage consists of two manual linear translation stages with metric micrometers (Daedal solid top model A37-936, 25 mm travel) and a motorized linear stage (National Aperture model MM-3M-EX-2.0, A55-329, 50.8 mm travel) coupled with a computer controller (National Aperture model MVP, A54-705) that allows the motion of the stage to be programmed using LabView. The injection system consists of an UltraMicroPump (UMP2) and a glass microvolume syringe (SGE50TLL) equipped with a silanized glass micropipette (Tip30TW1LS02), all obtained from World Precision Instruments. This injection system is operated using a microprocessor-based controller (UMC4) and is mounted on a manual micromanipulator (M3301). The image acquisition system in the drop motion experiments consists of two digital CMOS progressive scan monochrome cameras (Basler A601f, 1/2 in. sensor size with a firewire video output) connected through a PCI firewire card to a personal computer. The cameras are used to capture two orthogonal views of a moving drop from the side and the top. In static experiments used to measure the contact angle, a third identical digital camera that captures a view from another orthogonal direction also was employed. A light source (Dolan-Jenner PL-900) equipped with an IR filter is used to eliminate any potential heating of both the surface and the liquid drops during the performance of the experiments; temperature gradients can induce an uncontrolled, and therefore undesirable, thermocapillary contribution to the motion of the drop. An area fiber optic backlight (Edmund part number A54-228) is used to create uniform backlighting conditions to illuminate the side view.

Surface Preparation. Silicon wafers (4\P\100\B, prime grade) were obtained from Wafernet. AFM measurements showed that the surfaces of these wafers were smooth with an rms roughness of less than 0.2 nm. Strips of 35 mm × 30 mm with no visible scratches were cut from a silicon wafer and were cleaned using the following procedure: First, the strip was rinsed thoroughly with acetone, methanol, and DI (deionized) water and then placed in a megasonic bath containing DI water for 1 min to ensure the removal of any debris and particles on the strip surface. Next, the strip was dipped into a freshly prepared acid piranha solution (3:1 mixture of concentrated sulfuric acid (H_2SO_4) with 30% concentrated hydrogen peroxide (H_2O_2)) for 30 min and then rinsed thoroughly with DI water. Finally, the surface was dried with a jet of nitrogen and immediately used in the preparation of the gradient. The gradient was formed inside a desiccator. It is important to form the gradient under conditions of low relative humidity. When needed, a glovebox was used to lower the relative humidity in the environment to approximately 15%. A silk thread saturated with trichlorosilane was suspended above the edge of the strip for a period of up to 5 min. The chemical evaporates from the thread and diffuses along the silicon surface, reacting with its surface silanol groups. Locations on the surface that are closer to the thread become relatively more hydrophobic (less wettable). After forming the gradient, the strip was stored overnight inside the desiccator until the next day when the experiments on drop motion were performed.

In preparing the gradients, two different silanes (dodecyltrichlorosilane ($C_{12}H_{25}Cl_3Si$) and decyltrichlorosilane ($C_{10}H_{21}Cl_3Si$) from Gelest) were tried at different source heights, varying from 1.5 to 3.5 mm. It was found from contact angle measurements that the use of decyltrichlorosilane at a source height of 3.5 mm leads to a surface with the smallest gradient in the cosine of the contact angle; the largest gradient is obtained with dodecyltrichlorosilane at a source height of 1.5 mm. In most of the experiments reported here, the gradient was prepared using dodecyltrichlorosilane at a source height of 2.5 mm for an exposure time of 5 min. This leads to a gradient of the cosine of the contact angle that we label "intermediate." To test our approach for accommodating hysteresis effects, which is discussed in the Results and Discussion section, additional data obtained on a gradient surface formed using dodecyltrichlorosilane with a source height of 1.5 mm and an exposure time of 4 min (sharp gradient) and using dodecyltrichlorosilane with a source height of 3.5 mm and an exposure time of 5 min (gentle gradient) are also presented near the end and compared with predictions.

Measurement of Drop Velocities and Sizes. Drops of tetraethylene glycol (Sigma-Aldrich, 99%) of a range of nominal volumes from 50 to 2500 nL were each introduced on a separate unused migration path on the strip (hereafter called a track) near the beginning of the gradient region, and their motion was captured using the image acquisition system. The video frames were acquired at a rate of 50 frames/s. The positions of both the advancing and the receding ends of the migrating drop were tracked from one frame to the next using Spotlight-8 software.[23] Using both the side view and the top view, along with calibration information, the size of a drop and its position could be obtained from any given video frame. The instantaneous velocity at a given position was calculated as the local slope of a straight line fitted to a set of points chosen symmetrically about the selected position of the center of the drop's footprint on the position versus time curve. The number of points was chosen judiciously to minimize the error associated with scatter in the data if too few points are taken and the error associated with possible curvature in the data if too many points are chosen. In the first 2 mm of the gradient, seven points were chosen on each side of the position at which the velocity was being calculated; 16 points on either side were used from 2 to 5 mm, and 30 points on either side were employed from 5 mm to the end of the gradient. In the case of one of the drops that moved slowly between 6 and 10 mm, 50 points were used on each side.

Measurement of Static Contact Angles. It has been noted in refs 10 and 11 that sufficiently small drops do not move on a wettability gradient surface because of contact angle hysteresis. We found that drops that were less than 13 nL in volume (and 0.25 mm in footprint radius) did not move in the relatively gentle parts of the gradient surface. We therefore characterized the wettability gradient by making static contact angle measurements using such drops. The procedure adopted after considerable trial and error consisted of displacing a single small drop of the test liquid by small intervals along the gradient and capturing digital images from the side at a resolution of 1.2 μm/pixel. G-contact [24] software was then used to extract the shape of the drop, termed "profile" from hereon, from the image using Canny; the relative advantages and disadvantages of this method of extracting the profile when compared with those of other methods such as Sobel, Prewitt, and Laplacian of Gaussian (LOG) are discussed in depth in Bateni et al.,[25] who also provide guidelines on how best to obtain the contact angle from digitized images. We found that, as recommended by Bateni et al., fitting a third-degree polynomial to the profile near the contact line and obtaining the slope of the fitted polynomial where it intersects the solid surface gave the most stable results for the contact angles. Typically, it was necessary to use approximately 100 data points to fit the profile. Also, to eliminate the consequences of optical distortion in the region immediately adjacent to the contact line, about 13 μm of chord length (or approximately 13 data points beginning at the contact line) was removed.[26] In this manner, the contact angles at the front and the rear were obtained from the images of the drop at various locations along the gradient surface. We found that the drop was not absolutely stationary on the gradient surface in the region where the gradient was strong. A small amount of liquid was withdrawn from the drop to try to reduce the motion of the drop in this region so that its radius was approximately 0.2 mm; the velocity of the drop was sufficiently small (1−35 μm/s) for sharp images to be obtained for analysis. At locations where the gradient was not strong, the drop was indeed stationary for practical purposes.

(23) SpotLight is a software program written by R. Limek and T. Wright, NASA Glenn Research Center, Microgravity Science Division.

(24) G-Contact is a software program developed by J. De Coninck and coworkers from the University of Mons, Belgium.

(25) Bateni, A.; Susnar, S. S.; Amirfazli, A.; Neumann, A. W. *Colloids Surf., A* **2003**, *219*, 215.

(26) Marsh, J. A.; Garoff, S.; Dussan V., E. B. *Phys. Rev. Lett.* **1993**, 70, 2778.

Normally, on a homogeneous surface, a stationary drop should exhibit the same contact angle over the entire contact line. Because of the wettability gradient present on the experimental surface, one would expect the contact angle at the front to be smaller than that at the rear. Because the stationary drop used in characterizing the wettability gradient was small, we found that the difference in the measured contact angle between the front and the back of the drop was on the order of $\pm 1°$, which was the typical uncertainty in the contact angle measurement itself. Therefore, we averaged the values from the front and the back and assigned this average contact angle to the location of the center of the small drop. To test whether this was appropriate, we also measured, in selected cases, the contact angles at the two ends of the drop in an end view that was obtained in a direction parallel to the wettability gradient. In this view, which was obtained using an improved optical system, the contact angles at the left and right ends should be the same, in principle. We found in these experiments that the contact angles measured from the two ends again differed by up to $\pm 1°$ and, within this measurement error, were equal to the contact angles measured from the side view. We took this as justification for the protocol that the average of the values from the front and rear of the drop can be taken as the static contact angle at the location of the center of the drop's footprint. In this manner, graphs of the static contact angle (presumed to be the equilibrium value) and its cosine against position along the gradient were prepared. Each data set was fitted to a sigmoidal, logistic, four-parameter function for use in calculating the driving force and the hydrodynamic drag on the moving drops at various positions along the wettability gradient.

Theory

In the present experiments, the drops were sufficiently small for the gravitational deformation of their shapes to be negligible, and their motion was sufficiently slow for flow-induced deformation also to be negligible. The drops assumed a shape that could be fitted to a spherical cap, which is the shape assumed by a static drop in the absence of gravitational effects. Furthermore, the Reynolds number for the motion, defined in the Results and Discussion section, was found to be small compared with unity in all the experiments so that the flow within the drops can be assumed to be inertia-free. As noted in the Introduction, theoretical predictions for spherical cap drops moving in a wettability gradient have been obtained recently by Subramanian et al.[3] for the case of quasi-steady Stokes motion. Two principal results for the hydrodynamic resistance from that work are reproduced here. The first result is based on approximating the drop as a collection of wedges. In this case, the magnitude of the hydrodynamic force F_h exerted by the solid surface on the moving drop is given by

$$F_h = -8\mu U R\, f(\theta, \epsilon) \tag{1}$$

where

$$f(\theta, \epsilon) = \int_0^{1-\epsilon} \frac{(1 - Y^2)\tan^2\theta\left[\frac{1}{2}\ln(1 - Y^2) - \ln\epsilon\right]}{[\tan\theta\sqrt{1 - Y^2} - (1 + \{1 - Y^2\}\tan^2\theta)\tan^{-1}(\tan\theta\sqrt{1 - Y^2})]}\, dY \tag{2}$$

Here, μ is the viscosity of the liquid, U is the instantaneous velocity of the drop, R the radius of its footprint, θ is the dynamic contact angle formed by the spherical cap drop, assumed to be uniform around the contact line, and $\epsilon = L_s/R$, where L_s is the length of the region in which slip is permitted to occur. The integral in eq 2 must be evaluated numerically. An alternative analytical result, obtained using lubrication theory, also was given in reference 3. This result is given below.

$$F_h = 6\pi\mu U R[g(\theta, 0) - g(\theta, 1 - \epsilon)] \tag{3}$$

where

$$g(\theta, \xi) = \cot\theta \ln(\sqrt{\mathrm{cosec}^2\theta - \xi^2} - \cot\theta) + \sqrt{\mathrm{cosec}^2\theta - \xi^2} - \cot\theta \tag{4}$$

In writing the above results, we have made slight changes in notation from ref 3 for convenience. We note that the hydrodynamic resistance in eqs 1 and 3 can be written as

$$F_h = \beta U \tag{5}$$

where β is a resistance coefficient.

The driving force for the motion for a constant value of the gas−liquid surface tension γ is given in ref 3 as

$$F_{\text{driving}} = 2R\gamma\int_0^{\pi/2}\{\cos(\theta_e)_f - \cos(\theta_e)_r\}\cos\phi\, d\phi \tag{6}$$

Here, the integration is performed over the polar angle ϕ in a cylindrical polar coordinate system (r, ϕ) with its origin at the center of the drop's footprint. The ray corresponding to $\phi = 0$ points in the direction of the gradient. The symbol θ_e refers to the equilibrium contact angle, and the subscripts f and r correspond to front and rear, respectively. If the variation of the equilibrium contact angle along the gradient surface is known, then the integration required in eq 6 can be performed to obtain the driving force. In the present work, we fitted the measured static contact angles (assumed to approximate the equilibrium contact angle) along the gradient surface to a simple function of position and performed the integration numerically to obtain the driving force on a drop at any given location on the gradient surface. In estimating the parameter ϵ, we used a value of $L_s = 0.5$ nm. By equating the driving force and the hydrodynamic resistance, the quasi-steady velocity of the drop can be calculated.

The precise value of L_s, defined here as the length of the region near the contact line in which a slip model must be used, is not known. Discussions of the concept as well as the magnitude of L_s can be found in refs 27−29. For normal liquids and smooth surfaces, L_s is usually assumed to be on the order of the molecular size. Given the size of the liquid molecule used in the experiments and the estimate obtained from molecular dynamics simulations in ref 28 that $L_s \approx 1.8\sigma$, where σ is a Lennard-Jones parameter that can be assumed to be approximately the molecular diameter, we arrived at the estimate of $L_s = 0.5$ nm. In the next section, we provide an estimate of the sensitivity of the predicted hydrodynamic resistance to the value of L_s that is chosen.

Because the observed velocity of the drop changes with position along the gradient and therefore with time, one might wonder about the importance of unsteady-state effects. An approximate analysis of these effects can be found in ref 3, in which it is shown that, for a fixed driving force and a resisting force written in the form in eq 5, the time scale in which a drop of mass m is accelerated to its steady velocity is given by m/β. Under the conditions of the experiments, this time constant is found to vary from approximately 2×10^{-5} to 2×10^{-4} s. Furthermore, using the relevant physical properties of tetraethylene glycol and a typical length scale of the drop, the time scale for the viscous

(27) de Gennes, P. G. *Rev. Mod. Phys.* **1985**, *57*, 827.
(28) Thompson, P. A.; Brinckerhoff, W. B.; Robbins, M. O. *J. Adhes. Sci. Technol.* **1993**, *7*, 535.
(29) Kim, H.-Y.; Lee, H. J.; Kang, B. H. *J. Colloid Interface Sci.* **2002**, *247*, 372.

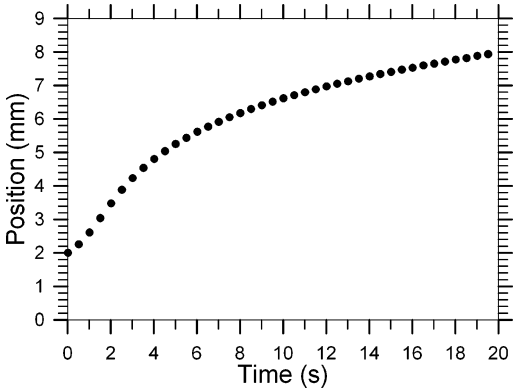

Figure 1. Position of a drop of nominal volume 500 nL plotted against the time of traverse.

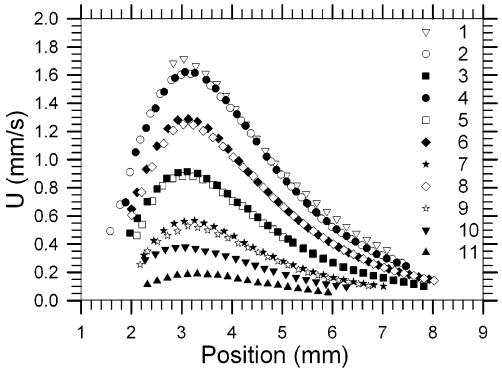

Figure 2. Velocities of several drops plotted against position on an intermediate gradient surface. The origin is chosen arbitrarily at the hydrophobic end where the contact angle is 70°, and the numbers assigned to the drops correspond to track numbers on the strip. The nominal volumes of the drops are 1 (2500 nL); 2, 4 (2000 nL); 3, 5 (500 nL), 6, 8 (1000 nL); 7, 9 (200 nL); 10 (140 nL); and 11 (50 nL).

drag to relax to its steady description in a transient analysis (R^2/ν, where ν is the kinematic viscosity of the liquid) can be estimated to be between 0.004 and 0.064 s. In the largest of these time scales, 0.064 s, the fastest drop would move approximately 0.12 mm, a distance in which the driving force and drag do not change appreciably. In view of this, it suffices to use a quasi-steady force balance to evaluate the theoretical prediction for the velocity of the drop at any given location on the gradient surface, and this is the procedure we follow in making predictions.

Results and Discussion

An important difference between the results of the present work and those presented in earlier studies[10,11] is the fact that we have measured the velocity of a given drop as a function of position. The trajectory of a typical drop on an "intermediate" gradient surface is shown in Figure 1. The inferred velocities of several drops, plotted as a function of position along the gradient, are displayed in Figure 2. The numbering of the drops corresponds to track numbers on the strip (i.e., adjacent numbers represent adjacent tracks). In Figures 1 and 2 and subsequent drawings in which experimental data are displayed, when the uncertainty in the measurement is not explicitly displayed, the uncertainty estimate is within the size of the symbols used. Also, the images were recorded at a frequency of 50 frames/s, but for clarity in the drawings, results are shown at 0.2 mm intervals in position.

It is seen from Figure 2 that the velocity of each drop rises to a peak in the first few millimeters and decays by as much as an order of magnitude as the drop moves into the more hydrophilic region on the strip. Figure 2 also demonstrates the reproducibility

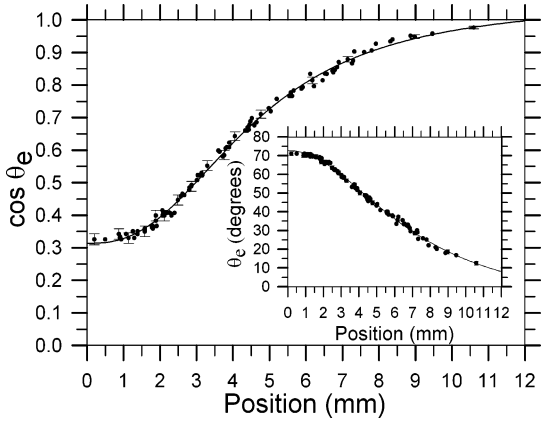

Figure 3. Cosine of the equilibrium contact angle θ_e plotted against position along the gradient surface. The solid curve shows the sigmoidal logistic function fitted to the data. The inset displays the angle θ_e plotted against position.

of the results on a given strip by comparing the behavior of drops of the same nominal volume introduced along different non-adjacent tracks on the gradient surface. The drop volume was varied from 50 nL for the smallest drop to 2500 nL for the largest drop. The radius of a given drop's footprint varies as it moves along the gradient and spreads out. The radius at the beginning of the motion varied from 0.33 to 1.33 mm, and that near the end of the motion varied from 0.44 to 1.71 mm. On the basis of these radius values and the measured velocities of the drops, it is possible to estimate a Reynolds number defined as $\mathrm{Re} = UR/\nu$, where ν is the kinematic viscosity of tetraethylene glycol at room temperature, which is 4.54×10^{-5} m^2/s. This Reynolds number varied from 5.13×10^{-4} to 5.05×10^{-2} in the experiments. Likewise, a capillary number can be defined as $\mathrm{Ca} = \mu U/\gamma$. Using a dynamic viscosity of $\mu = 5.11 \times 10^{-2}$ Pa·s and a surface tension of $\gamma = 46$ mN/m for tetraethylene glycol at room temperature, we estimate the range of values of the capillary number to be 5.9×10^{-5} to 1.9×10^{-3} in the experiments. The values of the Reynolds number are sufficiently small for the flow within the drops to be considered inertia-free, and those of the capillary number are sufficiently small for deformation caused by motion to be negligible, as mentioned earlier. Therefore, the drops should assume a shape close to their static shape. The Bond number, $\mathrm{Bo} = \rho g R^2/\gamma$, where $\rho = 1.13 \times 10^3$ kg/m^3 is the density of tetraethylene glycol at room temperature and $g = 9.81$ m^2/s is the magnitude of the acceleration due to gravity, varied from 0.027 to 0.70 in the experiments. This implies that the static shape of a drop on a homogeneous surface should be very close to that of a spherical cap. Of course, the drops are present on a gradient surface, where the equilibrium contact angle varies around the periphery of the drop. If this variation is considered to be sufficiently small, then the drops should assume the shape of a spherical cap as a first approximation. We found that the footprints of the drops in the experiments were well approximated by a circle and that the shapes of all of the drops from the side view could be fitted to an arc of a circle, confirming the validity of the spherical cap approximation to the shape of the moving drops.

Figure 3 shows the measured wettability gradient, plotted in the form of cos θ_e versus the position on the strip. An inset is used in this Figure to show the behavior of the angle θ_e with position along the gradient. For convenience in calculating the theoretical estimates of the driving force and resistance to motion, the data in the Figure were fitted to a sigmoidal, logistic, four-parameter function, which also is shown in Figure 3. It is evident from the Figure that the driving force is not uniform along the

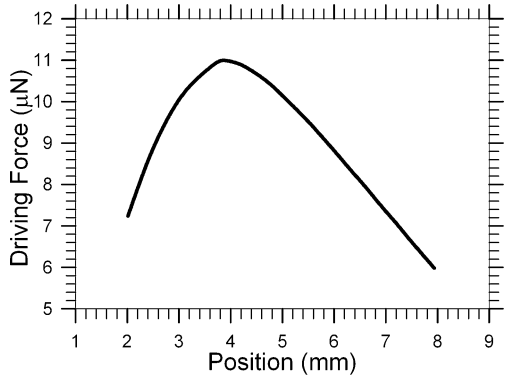

Figure 4. Driving force experienced by drop 5 plotted against position along the gradient surface.

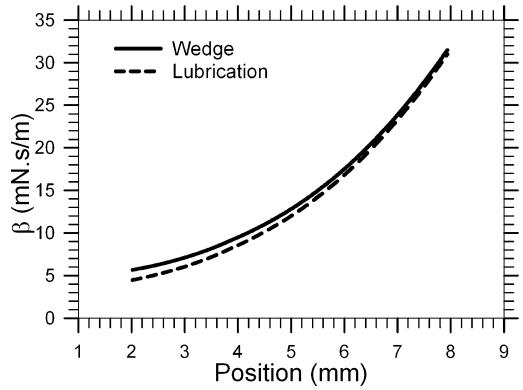

Figure 5. Hydrodynamic resistance coefficient β experienced by drop 5 plotted against position along the gradient surface. The solid line shows the resistance coefficient calculated from the wedge solution, and the dashed line corresponds to the resistance coefficient calculated from lubrication theory.

gradient surface, suggesting one reason for the variation of the velocity with position; the other is the fact that the local quasi-steady resistance coefficient changes continually as the drop moves along the strip. By resistance coefficient we mean coefficient β in eq 5. This change in β is caused by the change in the radius of the drop's footprint as well as the change in the dynamic contact angle; the ratio of the largest footprint radius to the smallest footprint radius is at most 1.3 so that a significant part of the change in β arises from its dependence on the contact angle. To demonstrate the extent of the variation in the driving force and the resistance along the gradient, we have chosen a representative drop of intermediate size in Figure 2 (drop 5, with a footprint radius of $R = 0.74$ mm when it begins moving). The driving force, calculated from eq 6 using the fitted result for the cosine of the equilibrium contact angle, is displayed in Figure 4 as a function of position along the gradient. Likewise, the magnitudes of hydrodynamic resistance coefficient β from the wedge approximation calculated from eqs 1 and 2 and that from lubrication theory calculated from eqs 3 and 4 are displayed in Figure 5.

In calculating the hydrodynamic resistance coefficient plotted in Figure 5, we used the equilibrium contact angle evaluated at the location of the center of the drop's circular footprint as the value of the dynamic contact angle of the moving drop. It is evident from Figures 4 and 5 that the driving force and the resistance coefficient vary substantially along the gradient surface. The driving force initially increases along the gradient surface, reaching a peak at a distance of roughly 4 mm, and then decreases to half that value near the end of the gradient. The coefficient β, evaluated from the wedge approximation, starts at a relatively

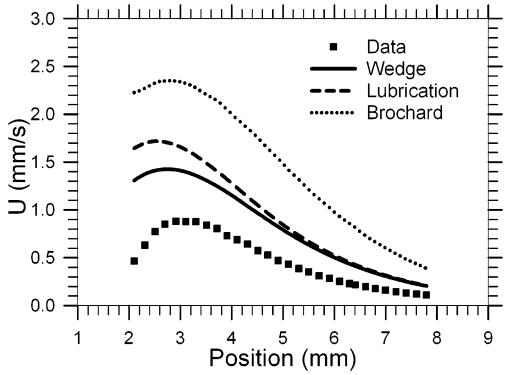

Figure 6. Comparison of the predicted and observed velocities of drop 5 plotted against position along the gradient surface. Shown are the data and the predictions from the wedge approximation, the lubrication theory solution, and the solution from Brochard.[4]

small value and increases by nearly a factor of 6 along the surface. As noted in ref 3, the resistance predicted from lubrication theory is observed to be smaller than that predicted by the wedge approximation but is nearly the same for positions at which the contact angles are less than or equal to about 40°. In calculating the results in Figure 5, the length of the slip region was assumed to be 0.5 nm. It is worth noting that the magnitude of the resistance coefficient is increased by approximately 10% when the length of the slip region is decreased to 0.1 nm, an extreme value; likewise, it is reduced by about the same extent when the length of the slip region is increased from 0.5 to 2 nm. This is a relatively small variation when compared with the nearly 6-fold change in the resistance coefficient over the gradient surface.

It is evident that the changes in the local driving force and the resistance coefficient are the reason for the spatial variation of the velocity of drop 5 observed in Figure 2. In Figure 6, we have compared the velocity obtained at each location by equating the local driving force and the resistance with the experimentally measured velocity for this drop. The comparison shows that the theoretical model approximately captures the behavior of the velocity as a function of position along the gradient surface. The wedge approximation yields a better prediction than lubrication theory. For comparison, we also have included the prediction from a result provided by Brochard[4] in the same Figure. It is seen that even though the wedge approximation does well in predicting the variation of the velocity with position, discrepancies remain between the predicted and observed values of the velocity. Similar discrepancies were noted when the data for the other drops were compared with the predictions from the best-performing theoretical model, namely, the wedge approximation, in Moumen's thesis.[30]

There are several reasons for the observed differences between the measured and predicted velocities. First, the theoretical prediction is approximate and not based on a complete numerical solution of the governing equations. Even a complete numerical solution would entail some approximation because it would require the use of some model of the slip region. As noted in ref 3, an exact solution should yield a larger predicted resistance than that from the wedge approximation, thereby moving the predicted velocities closer to the observed velocities. Second, the surface is assumed to be completely smooth in the model, and the roughness of the surface can contribute to increased resistance. Third, it is possible that dissipation at the contact line of the type envisioned in refs 14 and 15 can be important, contributing additionally to the resistance. Fourth, the theoretical

(30) Moumen, N. Motion of a Drop on a Horizontal Solid Surface with a Wettability Gradient. Ph.D. Thesis, Clarkson University, Potsdam, NY, 2006.

model assumes the shape of the drop to be that of a spherical cap, whereas the actual shape can be a bit different, being influenced both by gravitational and hydrodynamic effects. Finally, contact angle hysteresis can play a role in affecting the velocity of the drops. We had noticed when making contact angle measurements that drops that were sufficiently small did not move on the gradient surface. This fact also was recorded in refs 10 and 11, and Daniel and Chaudhury[10] actually suggested a method for accommodating the reduction in driving force caused by hysteresis using the idea of a "critical" drop size, which we shall term R_c. This is the footprint radius of a drop that is at the transition between drops that would move and those that would not at a given location on the gradient surface. For such a drop, one might postulate that the driving force is zero. The approach suggested by Daniel and Chaudhury[10] consists of using the driving force on a drop of footprint radius R_c as an additional form of resistance to be subtracted from the driving force on a given drop with $R > R_c$. We found that this yields a correction to the prediction that is too small, being proportional to R_c^2 when cos θ_e varies linearly with distance. Instead, we propose a different approach in which the cosine of the contact angle around the periphery of a drop of radius $R > R_c$ is reduced by the extent necessary to yield a zero driving force for a drop of critical radius R_c. This yields a correction that is proportional to RR_c when cos θ_e varies linearly with distance and therefore is larger, providing better agreement of the prediction with observation. Also, we found that the critical drop radius depends on the position along the gradient, and therefore accommodated this dependence. Details are given below.

Instead of using the equilibrium value of the contact angle around the periphery of the drop in eq 6, a reduced value for the receding portion of the contact line and an increased value for the advancing portion of the contact line must be used in evaluating the driving force corrected for hysteresis.

$$F_{\text{driving}} = 2R\gamma\int_0^{\pi/2}\{\cos\theta_f^{\text{hys}} - \cos\theta_r^{\text{hys}}\}\cos\phi\, d\phi \qquad (7)$$

If one imagines the drop's footprint to be divided into differential strips parallel to the direction of motion, then on each strip $\theta_f^{\text{hys}} = \theta_r^{\text{hys}}$ for the critical-size drop. Because the cosines of the measured equilibrium contact angles at the front and rear can be evaluated over the periphery of the critical-sized drop, this provides a quantitative estimate of the correction over the advancing portion of the contact line, $[\cos(\theta_e)_f - \cos\theta_f^{\text{hys}}]$, and that over the receding portion of the contact line, $[\cos\theta_r^{\text{hys}} - \cos(\theta_e)_r]$, at the position on the gradient surface where the drop is located. This concept is illustrated graphically in the sketch in Figure 7 in which locally linear behavior of the plot of cos θ_e versus x has been assumed.

The solid line in Figure 7 represents the equilibrium contact angle at each position. The two dashed lines above and below it, located such that their horizontal distance from the solid line is R_c, provide plots of $\cos\theta_r^{\text{hys}}$ versus position and $\cos\theta_f^{\text{hys}}$ versus position, respectively. Thus, to obtain the difference $\{\cos\theta_f^{\text{hys}} - \cos\theta_r^{\text{hys}}\}$ along each differential strip of the footprint of a given drop (parallel to the direction of motion), one would, in effect, use the curve of $\cos(\theta_e)$ versus position but evaluate this function at the periphery of an imaginary drop of radius $R - R_c$. Of course, to make this revision in the driving force, one must know the critical size at different locations along the gradient surface. For this purpose, we selected a few locations along the surface where the velocities of drops of various sizes had been measured and plotted the velocity as a function of drop radius at each location, as shown as Figure 8.

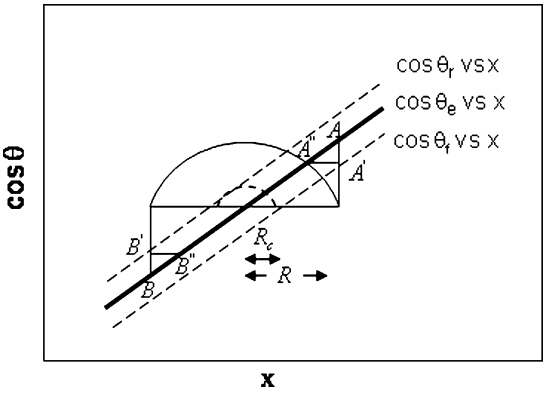

Figure 7. Sketch showing how the effect of hysteresis can be accommodated by evaluating the difference $[\cos(\theta_e)_f - \cos(\theta_e)_r]$ around the periphery of an imaginary drop of radius $R - R_c$. The ideal driving force is the difference between the ordinates of A and B; the reduced driving force is the difference between the ordinates of A' and B', which is the same as the difference between the ordinates of A'' and B'', which correspond to the equilibrium contact angles for a drop of radius $R - R_c$ at the given location. Shown in the sketch is the section of the drop in the symmetry plane; at other sections, similar reasoning applies, but the horizontal distances from the location of the center of the drop become $(R - R_c)\cos\phi$.

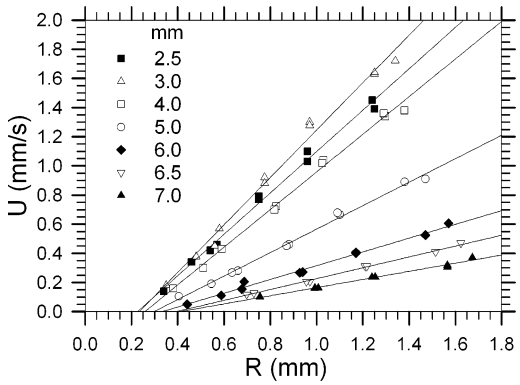

Figure 8. Velocities of drops plotted as a function of footprint radius at several selected positions along the gradient. Also shown in each case are the best-fit straight lines.

It is seen from Figure 8 that the velocity scales approximately linearly with drop size, which is consistent with theory[3] because the factor ln ϵ that appears in the theoretical result does not change substantially over the range of drop radii employed. We fitted the set of data for a given position to a straight line and used the intercept on the x axis (where the velocity is zero) as the critical radius R_c for that location. A graph showing the behavior of R_c, obtained by this method, against position is displayed as Figure 9, along with a curve that represents a cubic function that was used to fit these data, so that we could calculate interpolated values of R_c at any desired location. Then, the driving force corrected for hysteresis was evaluated using the scheme explained above.

In Figure 10, we have compared the data on the velocity of drop 5 as a function of position with two modified predictions and also included the prediction from the wedge approximation with the unmodified driving force for comparison. One of the modified predictions corresponds to evaluating the hysteresis effect as recommended by Daniel and Chaudhury,[10] and the other corresponds to the present approach to correcting for hysteresis described using Figure 7. The comparison demonstrates that the present approach performs remarkably well in closing the gap between the predicted and observed velocities.

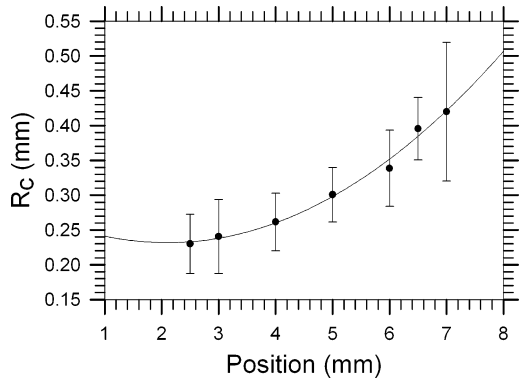

Figure 9. Critical drop radius R_c plotted as a function of position along the gradient surface. Also shown is the cubic fit that was used for the purpose of interpolation.

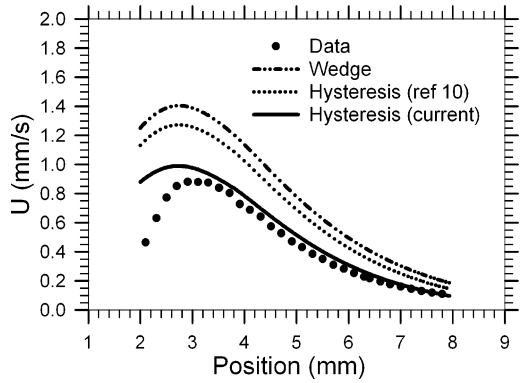

Figure 10. Comparison of predicted and observed velocities of drop 5 plotted against position along the gradient surface. Shown are the data and the predictions from the wedge approximation with the original driving force, the wedge approximation with the driving force corrected for hysteresis using the approach in ref 10, and the wedge approximation with the driving force corrected for hysteresis using the present approach.

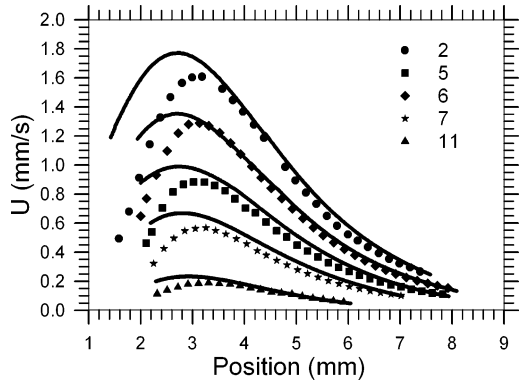

Figure 11. Comparison of predicted and observed velocities of several drops. The solid curves represent predictions made using the wedge approximation and a driving force modified using the present approach to accommodate the effect of hysteresis.

In Figure 11, we have plotted the data on drop velocity as a function of position for several drops along with the modified prediction from the wedge approximation, using the present approach for correcting the driving force. To avoid clutter, we have eliminated some of the drops in presenting this Figure, but the extent of agreement is comparable for the excluded drops as noted in ref 30. The improved agreement between the data and the modified prediction suggests that the hypothesis that the driving force indeed is reduced due to

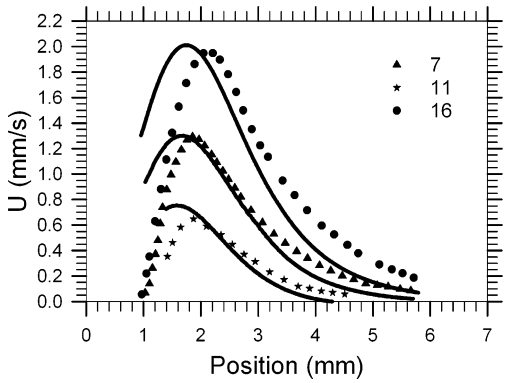

Figure 12. Sharp gradient: comparison of predicted and observed velocities of selected drops. The solid curves represent predictions made using the wedge approximation and a driving force modified using the present approach to accommodate the effect of hysteresis. The numbers assigned to the drops correspond to track numbers on the strip. The nominal volumes of the drops are 7 (150 nL), 11 (50 nL), and 16 (500 nL).

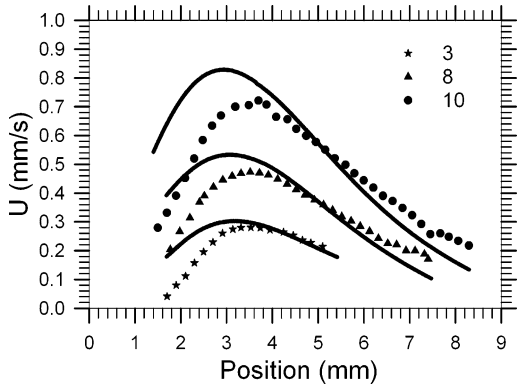

Figure 13. Gentle gradient: comparison of predicted and observed velocities of selected drops. The solid curves represent predictions made using the wedge approximation and a driving force modified using the present approach to accommodate the effect of hysteresis. The numbers assigned to the drops correspond to track numbers on the strip. The nominal volumes of the drops are 3 (500 nL), 8 (1000 nL), and 10 (2000 nL).

hysteresis is viable in explaining the behavior of the drops on the gradient surface.

We also attempted other ways, described in ref 30, of explaining the discrepancy between the data and the unmodified prediction from the wedge approximation. These attempts involved modifying the resistance by assuming that there exists additional resistance to the motion that is proportional to either the drop velocity or the product of the drop velocity and drop radius (as is true of the hydrodynamic model or one based on contact line resistance). We then extracted a coefficient for this additional resistance by requiring the data on an intermediate-sized drop to match the revised prediction. Then, using this additional resistance coefficient as a function of position along the gradient surface, we attempted to predict the velocity versus distance behavior for all the other drops. Although reasonably successful, this attempt did not lead to the level of agreement of the predicted and observed velocities that is noted in Figures 10 and 11. The best agreement was obtained when we used the idea of an additional resistance that was independent of drop radius or velocity, but this is precisely the type of correction provided by the hysteresis model used in modifying the driving force in Figure 10. Therefore, it appears that the discrepancy between the uncorrected predictions and the data in the present experiments is more likely due to a reduction in the driving force rather than

an additional resistance arising either from a hydrodynamic origin or from contact line dissipation of the form envisioned in refs 14 and 15. The agreement between the observed and predicted velocities in Figure 11 is not perfect, especially during the early part of the traverse, and the remaining differences may be due to a variety of reasons discussed earlier, also including the fact that we can only approximately accommodate the hysteresis effect.

As noted in the subsection on Surface Preparation, the gradient used in the above experiments is termed intermediate. To test whether the theoretical model from ref 3, modified to accommodate hysteresis effects as outlined here, is able to predict the behavior of drops in other experiments, experiments were also performed using "sharp" and "gentle" gradient surfaces; these terms are defined in the subsection on Surface Preparation. Results obtained from these experiments for the velocities of drops of different sizes as a function of position along the gradient surface are presented in Figures 12 and 13 and compared with the predictions from the wedge model from ref 3, corrected for hysteresis effects in the manner outlined here. It appears that the present approach does a reasonable job of predicting the velocities of the drops in these experiments as well. Additional results are presented and discussed in Moumen's doctoral thesis.[30]

Concluding Remarks

Detailed measurements of the velocity of a drop along a wettability gradient surface reveal the complex nature of the variation of the velocity in response to the change in driving force and in the resistance to the motion of the drop along the gradient. We demonstrate that it is possible to interpret and organize the results using a simple hydrodynamic model in which inertial effects and deformation due to gravity as well as motion are neglected. The predictions from the wedge approximation describe the qualitative features of the shape of the curve of velocity versus position along the gradient surface, and the quantitative differences are mostly accommodated by approximately accounting for the influence of hysteresis on the motion of the drops.

Acknowledgment. We thank Professor M. K. Chaudhury and Dr. S. Daniel, Lehigh University, for their help in training N.M. in the technique for the preparation of the gradients and for helpful advice and comments. Also, we thank E. Rame of the NASA Glenn Research Center and S.S. Suppiah of Clarkson University for numerous helpful discussions. This work was supported by NASA grant NAG3-2703.

LA053060X